Nanoscale

Accepted Manuscript

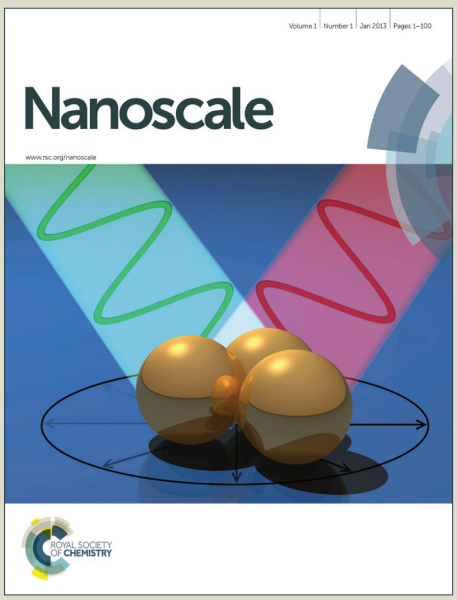

ROYAL SOCIETY OF CHEMISTRY

www.rsc.org/nanoscale

Cite this: DOI: 10.1039/c0xx00000x

www.rsc.org/xxxxxx

ARTICLE TYPE

Electrical control of memristance and magnetoresistance in oxide magnetic tunnel junctions

Kun Zhang,[a] Yan-ling Cao,[a] Yue-wen Fang,[b] Qiang Li,[a] Jie Zhang,[a] Chun-gang Duan,[b] Shi-shen Yan,*[a] Yu-feng Tian,*[a] Rong Huang,[b] Rong-kun Zheng,[c] Shi-shou Kang,[a] Yan-xue Chen,[a] Guo-lei Liu,[a] and Liang-mo Mei[a]

Received (in XXX, XXX) Xth XXXXXXXXX 20XX, Accepted Xth XXXXXXXXX 20XX
DOI: 10.1039/b000000x

Electric-filed control of magnetic and transport properties of magnetic tunnel junctions has promising applications in spintronics. Here, we experimentally demonstrate a reversible electrical manipulation of memristance, magnetoresistance, and exchange bias in Co/CoO-ZnO/Co magnetic tunnel junctions, which enables the realization of four nonvolatile resistance states. Moreover, greatly enhanced tunneling magnetoresistance of 68% was observed due to the enhanced spin polarization of the bottom Co/CoO interface. The *ab* initio calculations further indicate that the spin polarization of Co/CoO interface is as high as 73% near the Fermi level and plenty of oxygen vacancies can induce metal-insulator transition of CoO_{1-v} layer. Thus, the electrical manipulation mechanism on the memristance, magnetoresistance and exchange bias can be attributed to the electric-field-driven migration of oxygen ions/vacancies between very thin CoO and ZnO layers.

1. Introduction

Information storage and communication technology require solutions for further miniaturization, lower power consumption, and multifunctionality, which relies on the development of new materials and novel device concepts. A realistic approach to meet such demands is the electrical control of the magnetic and transport properties,[1-3] which is of great interest not only for technological applications but also for fundamental physics. By introducing capacitive charge accumulation at the interface, electric field could modify the density of states at the Fermi level, which further lead to the manipulation of magnetism and magnetic anisotropy.[4,5] By reversing the ferroelectric polarization of insulating barrier, electric field could tune the tunneling barrier height/width of a ferroelectric magnetic tunnel junctions (MTJs), which further lead to the manipulation of magnetoresistance (MR).[6-9] By charge transfer and orbital reconstruction, electric field control of exchange bias could be achieved.[10] Furthermore, by changing the carrier distribution, electronic barrier height and the oxidation state of a ferromagnet, electric-field-induced ion electromigration could lead to various emergent phenomena, such as electrical resistive switching, interfacial ferromagnetism and exchange bias.[11-14]

It would be an important step towards multifunctional spintronics if multiple physical properties can be electrically tuned simultaneously. It is well known that oxygen vacancies (O_v) in many oxides are intrinsically coupled with magnetic, electronic and transport properties.[15] Therefore, in principle, electrical-field-driven oxygen vacancy/ion migration in oxide MTJs may greatly change the electronic band structure and even the ion oxidation states of the oxides, opening pathways for simultaneous electrical manipulating of memristance, magnetoresistance, and exchange bias. In fact, binary transition metal oxides such as NiO, TiO_2, and CoO have been widely studied as memristance materials,[16,17] where remarkable electrical control of resistance can be achieved, but they are hard to obtain large magnetoresistance as the insulating layer in MTJs. By contrast, the insulating barrier of MTJs with large tunneling magnetoresistance (TMR) is usually limited to very few oxides, such as Al_2O_3, MgO, and HfO_2,[18] where junction resistance is hard to be electrically tuned in a reversible way.

Recently, our group proposed to use nano-composite barrier of CoO-ZnO to fabricate the spin memristive Co/CoO-ZnO/Co MTJs, where three resistance states were obtained.[19] In this paper, we experimentally demonstrate the realization of four nonvolatile resistance states in Co/CoO-ZnO/Co magnetic tunnel junctions and the simultaneous electrical manipulation of memristance, magnetoresistance, and exchange bias. The *ab* initio calculations further indicate that the spin polarization ratio of tunneling electrons at Co/CoO interface is greatly enhanced up to 73.2% due to *s,p-d* hybridization, which can well explain the experimentally observed large TMR of 68% at 5 K.

2. Materials and Methods

2.1 Sample Preparation

The glass/Cr(2 nm)/Ag(30 nm)/Co(10 nm)/CoO-ZnO(2 nm)/Co(30 nm)/Ag(60 nm) MTJs with an area of 0.1mm × 0.1mm were deposited by a magnetron sputtering machine with a base pressure of 6×10^{-8} Torr using shadow masks. A thin layer

of Cr was grown to enhance the attachment of the bottom Ag electrode on the glass substrate. The bottom Co layer of 10 nm was deposited under an Ar gas of 5 × 10^{-3} Torr. Then a semiconducting ZnO layer of 2 nm was deposited by RF reactive sputtering of ZnO target under the argon-oxygen mixture of 6 × 10^{-3} Torr with 0.3% oxygen ratio. An antiferromagnetic insulating CoO thin layer was produced on the surface of the bottom Co layer during the deposition of ZnO. Finally the top 30 nm Co layer with 60 nm Ag electrode was grown at a high Ar pressure of 1.5 × 10^{-2} Torr, resulting in a larger coercivity (H_C = 310 Oe) at room temperature than that of the bottom Co layer (H_C = 70 Oe) grown at lower pressure.

2.2 Physical Characterization

The electrical transport measurements were carried out in a four-point configuration in a Quantum Design instrument with the Model 2400 source meter and Model 2182A nano voltmeter. The bottom and top electrode contact resistance is negligible as compared with the junction resistance, which eliminates the current crowding. The magnetic properties were characterized with a SQUID magnetometer. The temperature is in a range from 2 to 300 K, and the magnetic field is up to 7 T. Low-magnification and High resolution cross-section transmission electron microscopy (TEM) images of samples were performed with a JEOL 2200FS microscope. Typically the images were acquired at an accelerating voltage of 200 kV.

2.3 Calculation methods

All spin-polarized *ab* initio calculations were performed using density functional theory codes implemented in Vienna *ab* initio simulation package (VASP)[20] with projector augmented wave (PAW) pseudopotentials. We applied GGA plus Hubbard U approach to take into account the on-site repulsion of localized Co-3d orbitals, employing the Dudarev[21] method with an effective value of Ueff = 6.1 eV for cobalt atoms[22] in bulk CoO and interfacial cobalt atoms throughout our calculations. For optimization, we fixed the in-plane atomic positions while fully relaxed the atomic positions along *c*-direction perpendicular to the interface until the Hellmann-Feynman forces on each atom are less than 1 meV/Å. Relaxation and self-consistent calculations are both performed using a plane-wave basis set limited by a cutoff energy of 600 eV and the 5×5×1 Γ-centered grids.

3. Results and discussion

3.1 Microstructure and valence states of Co in Co/CoO-ZnO/Co MTJs

The cross-section images of Co/CoO-ZnO/Co MTJs were observed by TEM. The low-magnification and high resolution TEM images in Fig.1A and Fig.1B indicate that the interfaces of Co/CoO-ZnO/Co MTJs are quite sharp and clean. Also, different lattice fringes are observed, suggesting that the individual sublayers of the MTJs are in the nanocrystalline state. In order to quantify the local valence states of Co, the electron energy loss spectroscopy (EELS) is measured at three different regions, as marked by regions 1, 2 and 3 in Fig. 1B. Fig. 1C shows a direct comparison of the Co L-edges for the above three regions. A lower energy tail and a narrower L_2 edge in region 2 compared with region 1 (pure Co) are observed, which is consistent with the strongly oxidized CoO_{1-v} in region 2.[23] For the same reason, region 3 only shows weakly oxidized CoO_{1-v}.

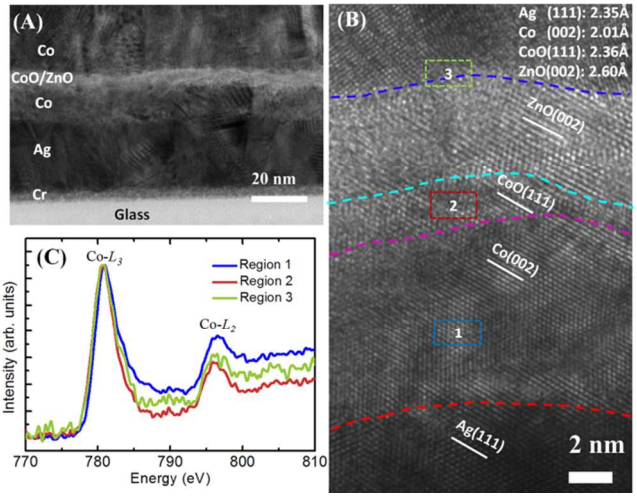

Fig. 1. Microstructure and valence states of Co in the Co/CoO-ZnO/Co MTJs. (A) Low-magnification cross-section TEM image of the glass/Cr (2 nm)/Ag (30 nm)/(Co 10 nm)/CoO-ZnO (3 nm)/Co(30 nm)/(Ag 60 nm) MTJs, where the Cr layer is the buffer layer, and the two Ag layers are electrodes. (B) High resolution TEM image. The dashed lines are guides to the eyes to show the interface boundaries. (C) The EELS of Co L-edges measured at three different regions as labeled in (B).

3.2 Electrical resistive switching and magnetoresistance

Fig. 2A shows the current-voltage (I-V) characteristic of the MTJ measured at 300 K, where a clear electrical bistability is observed. The I-V curve is initially nonlinear in the as-grown junction, which indicates a tunneling transport in the high resistance state (HRS), while it is linear in the low resistance state (LRS), which suggests a metallic transport behavior. The resistance ratio of HRS to LRS is 40 around zero voltage. Moreover, this electrical manipulation of the bipolar resistive switching is reversible and reproducible.

Fig. 2B and Fig. 2C exhibit one of the most intriguing and innovative part of current investigation, i.e., the intimate interplay between the resistive switching and magnetoresistance. As shown in Fig. 2B and Fig. 2C, the MR of HRS and LRS at 300 K is, respectively, 15.2% and 2.5%. Here, MR is defined as MR= $(R_{AP}-R_P)/R_P$, where R_{AP} and R_P are the resistance of the junction when the magnetization of two Co layers is antiparallel and parallel to each other. Figure 3 further shows the temperature dependence of the junction resistance at HRS, where semiconducting/insulating behavior is observed, i.e., junction resistance increases with decreasing temperature. Together with the nonlinear I-V curve of the HRS, the observed MR in HRS is attributed to TMR effect.[24] On the other hand, at LRS linear I-V curves is obtained as shown in Fig. 2(A), suggesting that Ohmic transport plays the dominate role and tunneling process could be neglected. Hence, the MR in LRS is attributed to current-perpendicular-to-plane giant magnetoresistance (CPP-GMR) effect.[25] Therefore, combining TMR effect in the HRS and GMR effect in the LRS, 4 nonvolatile resistance states were obtained in

Co/CoO-ZnO/Co junctions. Since the Néel temperature of bulk CoO is 293 K,[26] no exchange bias effect was found in Fig. 2B at 300 K.

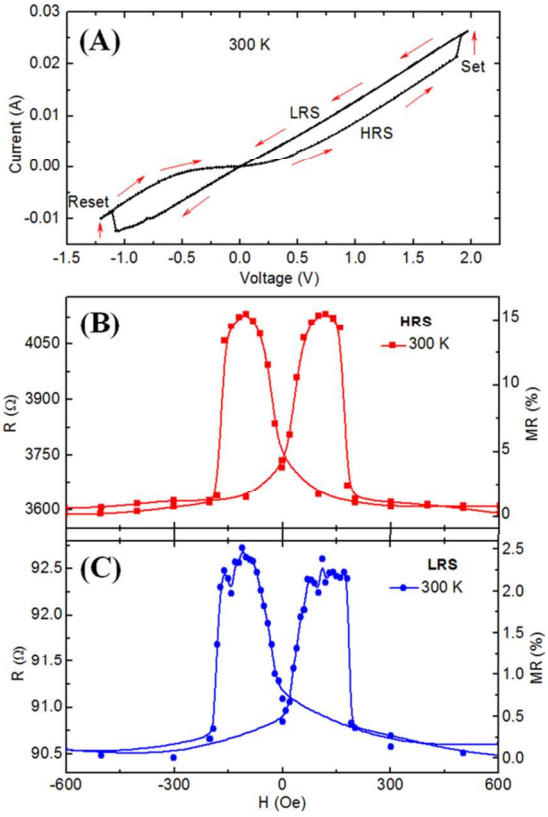

Fig. 2. Electrical resistive switching and magnetoresistance of the Co/CoO-ZnO/Co MTJs. (A) The I-V curve of memristance, (B) magnetoresistance curve in the high resistance state, and (C) magnetoresistance curve in the low resistance state.

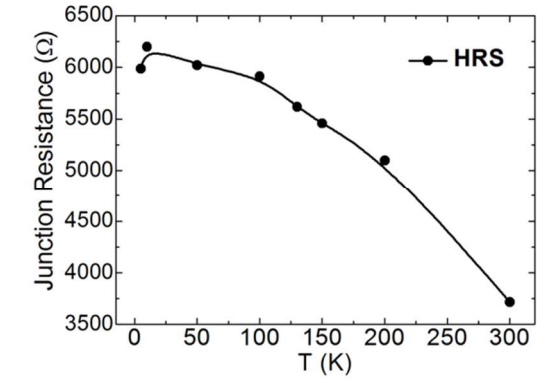

Fig. 3. The temperature dependence of the junction resistance at HRS.

3.3 Enhanced TMR and electrically controllable exchange bias

To make the story more interesting, we find that TMR at low temperature is greatly enhanced and the exchange bias can be electrical programmable, which is revealed in Fig. 4A and Fig. 4B. The low temperature MR was measured at 5 K after magnetic field (30000 Oe) cooling from 300 K. The maximum TMR is 68% in the HRS at 5 K as shown in Fig. 4A, and it still remains 15.2% at 300 K as shown in Fig. 2B. But the magnitude of GMR in the LRS almost keeps unchanged (2.5%) from 300 K to 5 K as shown in Fig. 2C and Fig. 4B. Within Jullière model,[24] the magnitude of TMR is determined by the spin polarization of the tunneling electrons, $TMR=(R_{AP}-R_P)/R_P=2P_1P_2/(1-P_1P_2)$, where P_1 and P_2 are the spin polarization ratios of tunneling electrons at free and pinned electrodes, respectively. Assuming the spin polarization $P_1=P_2=35\%$ for both Co metal layers,[27] the theoretical value of TMR predicted by Julliére model is only 28%. In this sense, our experimental TMR of 68% in the HRS is greatly enhanced at low temperature.

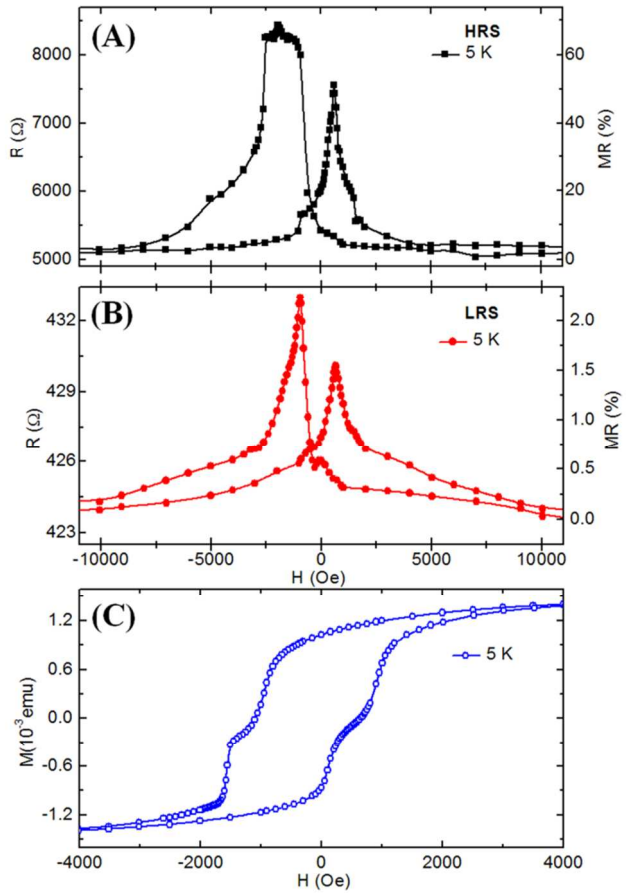

Fig. 4. Magnetoresistance and exchange bias. Magnetoresistance curve in the high resistance state (A), and the low resistance state (B) of the Co/CoO-ZnO/Co MTJs measured at 5 K. (C) The M-H loop of the same junctions but larger area of 5 mm × 5 mm measured at 5 K. All the measurements were carried out after the samples were cooled down from 300 K to 5 K in a magnetic field of 30000 Oe.

On the other hand, comparing Fig. 4 with Fig. 2, we find that the resistance in Fig. 4 has robust asymmetric dependence on the magnetic field. Not only the maximum peak resistance is different for the positive and negative magnetic field branch, but also the positions of the peak resistance are shifted to the negative magnetic field, indicating a significant exchange bias effect. This

kind of asymmetric behavior is believed to be intrinsic to the exchange biased systems due to different magnetization reversal pathways at each branch of the hysteresis loop,[28] such as domain wall motion at the positive magnetic field but coherent rotation at the negative magnetic field. Here, the effective exchange bias field is defined as $H_E=(H_+ + H_-)/2$, where $H_+(H_-)$ is the location of positive (negative) resistance peak. The effective coercivity field is then defined to be half the distance between the two peaks $H_C=(H_+ - H_-)/2$. The deduced H_E in the HRS is 670 Oe while it is 160 Oe in the LRS. Meanwhile, H_C is changed from 1270 Oe in the HRS to 800 Oe in the LRS. This unambiguously illustrates that the interfacial exchange coupling strength is greatly modulated by the electrical resistive switching. However, in our case, the exchange bias effect disappears above 100 K, suggesting that the very thin CoO layer of ~2nm formed at the Co surface may have a Néel temperature about 100 K, which is obviously lower than 293 K of bulk CoO.[26] The existence of exchange bias is further confirmed by the M-H loop as shown in Fig. 4C, which is caused by the interfacial exchange coupling between the bottom ferromagnetic Co layer and the antiferromagnetic CoO_{1-v} layer.

3.4 *ab* initio calculations on Co/CoO/Co junctions

In the following, combining with the *ab* initio calculations, we explore the physical mechanisms responsible for the electrical manipulation of memristance, exchange bias, and enhanced MR. In our Co/CoO-ZnO/Co junctions with CoO-ZnO composite insulating layers, ZnO in the form of ZnO_{1-v} is a natural *n*-type semiconductor due to the existence of oxygen vacancies, which has very small resistivity as compared with insulating CoO. Meanwhile, in our oxygen-deficient case, CoO in the form of CoO_{1-v} has a trend to become more insulating by obtaining oxygen ions. If the applied electrical field can drive the oxygen vacancies/ions to migrate between very thin CoO and ZnO layers, it may simultaneously realize the electrical manipulation of memristance, MR, and exchange bias in the MTJs.

To shed light on the critical role played by oxygen vacancies, we performed *ab* initio calculations on Co/CoO/Co junctions with/without oxygen vacancies in the interlayer CoO. In order to simulate the experimentally observed structure, we constructed an ideal Co(002)/CoO(111)/Co(002) structure model in a hexagonal cell as shown in Fig. 5A. As a comparison, a defected Co/CoO/Co structure with 25% oxygen vacancy concentration was simulated by removing oxygen atoms symmetrically with respect to the center of unit cell in the ideal model for the purpose of avoiding long-range dipole interactions between periodic images and reducing computing time technically. In these initial models, the type-II antiferromagnetic ordering of interlayer CoO was satisfied to form uncompensated CoO surfaces alone [111] direction.

3.5 Insulating antiferromagnetic CoO layer

Fig. 5B shows the density of states (DOS) of interlayer CoO in the ideal Co/CoO/Co junctions. It is clear that CoO interlayer is an antiferromagnetic Mott-insulator with the band gap about 2.0 eV. This means that our experimentally prepared Co/CoO-ZnO/Co junctions should be in a high resistance state and show tunneling transport if the CoO layer is a good insulator. Meanwhile, it is natural that the antiferromagnetic insulating CoO layer can produce a significant exchange bias on the bottom ferromagnetic Co layer.

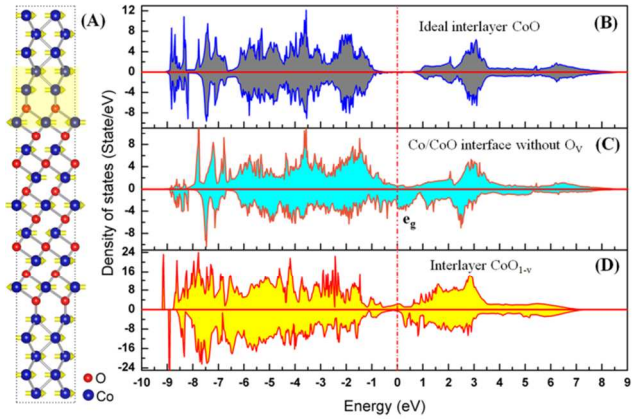

Fig. 5. *ab* initio calculation results of Co/CoO/Co junctions. (A) The schematics of the atomic configuration in ideal Co/CoO/Co junctions, where the Co/CoO interface with Co-Co-O-Co four atomic layers is marked by the yellow area and the spin direction is shown by the yellow arrows. The density of states of the interlayer CoO without oxygen vacancies (B), the Co/CoO interface without oxygen vacancies (C), and the interlayer CoO_{1-v} with the oxygen vacancy concentration v=0.25 (D). The dashed line indicates the Fermi level.

3.6 Enhanced spin polarization of Co/CoO interface

Fig. 5C shows the DOS of Co/CoO interface with Co-Co-O-Co four atomic layers in the ideal Co/CoO/Co junctions. It is very interesting that though overall CoO layer is an ideal insulator as shown in Fig. 5B, the Co/CoO interface in Fig. 5C becomes metallic and has a very high spin polarization ratio of 73.2% near the Fermi level due to strong *s,p-d* hybridization at the interface, in particular, Co e_g orbitals contribute a lot to the DOS at the Fermi level.

According to Julliére model,[24] assuming P_2=35% for the top ZnO/Co interface, we derived P_1=72% for the bottom Co/CoO interface from TMR=68% in our Co/CoO-ZnO/Co junctions, which is in well agreement with the theoretical spin polarization of 73.2% at Co/CoO interface. Therefore, the enhanced TMR in our Co/CoO-ZnO/Co junctions can be attributed to the enhanced spin polarization of the bottom Co/CoO interface. Beside high spin polarization,[29] spin filter[30] and Coulomb blockade effects[31] can also enhance TMR for some specific MTJs structures, but the later two are easily excluded in our case.

3.7 Metal-insulator transition caused by electromigration of oxygen vacancies

Fig. 5D shows the DOS of defected interlayer CoO_{1-v} in the $Co/CoO_{1-v}/Co$ junctions with the oxygen vacancy concentration v=0.25. It is clear that though CoO is a good insulator, interlayer CoO_{1-v} in the $Co/CoO_{1-v}/Co$ junctions with enough oxygen vacancies becomes metallic and has a spin polarization ratio of 66.9% near the Fermi level.

As for our case, the as-prepared Co/CoO-ZnO/Co junctions are in a HRS due to the existence of insulating CoO. Under a positive

bias voltage, oxygen ions (O^{2-}) can migrate from the CoO_{1-v} layer to the ZnO_{1-v} layer, which produces more oxygen vacancies in CoO_{1-v}. According to Fig. 5D, with increasing concentration of oxygen vacancies, metal-insulator transition occurs in CoO layer. Hence, our experimentally prepared Co/CoO-ZnO/Co junctions change into the LRS and show metallic transport. Meanwhile, according to Fig. 5D, oxygen vacancies in CoO_{1-v} layer can weaken and even destroy the antiferromagnetism of CoO, so the exchange bias field is sharply reduced in the low resistance state. Finally, it should be pointed out that though the metallic CoO_{1-v} can show a high spin polarization ratio of 66.9% in the LRS, the MR in diffusive transport is still low because of the fundamental conductivity mismatch between the ferromagnetic metal Co/CoO_{1-v} layers and the semiconducting ZnO_{1-v} layer.[32]

4. Conclusions

In conclusion, we have demonstrated that the memristance, magnetoresistance, and exchange bias field can be electrically manipulated to obtain four nonvolatile resistance states in Co/CoO-ZnO/Co junctions. Moreover, Co/CoO-ZnO/Co MTJs can show greatly enhanced TMR of 68%, which can be well explained by the enhanced spin polarization of the bottom Co/CoO interface due to strong *s,p-d* hybridization. The electrically manipulated MTJs offer new possibility toward multiple states nonvolatile storage.

Acknowledgements

Y.W. Fang appreciates useful discussions with U.D. Wdowik of Pedagogical University, S. Grytsyuk from KAUST and Prof. Marie-Liesse Doublet from CNRS. This work was supported by the key program of NSFC No. 11434006, the NBRP of China No. 2013CB922303 and 2014CB921104, the NSF for Distinguished Young Scholars of China (No.51125004), 111 project No. B13029, and NSFC No. 11374187 and 61125403.

Notes and references

[a] *School of Physics, State Key Laboratory of Crystal Materials, Shandong University, Jinan, 250100, P. R. China. E-mail: shishenyan@sdu.edu.cn* and *yftian@sdu.edu.cn*

[b] *Key Laboratory of Polar Materials and Devices, Ministry of Education, East China Normal University, Shanghai, 200062, P. R. China.*

[c] *Australian Center for Microscopy & Microanalysis, University of Sydney, Sydney, NSW 2006, Australia.*

† Electronic Supplementary Information (ESI) available: [details of any supplementary information available should be included here]. See DOI: 10.1039/b000000x/

1. R. Waser and M. Aono, *Nature Mater.*, 2007, **6**, 833.
2. W. G. Wang, M. Li and C. L. Hageman, *Nature Mater.*, 2012, **11**, 64.
3. C. G. Duan, J. P. Velev, R. F. Sabirianov, Z. Zhu, E. Y. Jaswal, and E. Y. Tsymbal, *Phys .Rev. Lett.*, 2008, **101**, 137201.
4. M. Weisheit, S. Fahler, A. Marty, Y. Souche and C. Poinsignon, *Science*, 2007, **315**, 419.
5. T. Maruyama, T. Shiota, K. Nozaki, N. Ohta, N. Toda, M. Mizuguchi, A. A.Tulapurkar, T. Shinjo, M. Shiraishi, S. Mizukami, Y. Ando and Y. Suzuki, *Nature Nanotech.*, 2009, **4**, 158.
6. V. Garcia, M. Bibes, L. Bocher, S. Valencia, F. Kronast, A. Crassous, X. Moya, S. Enouz-Vedrenne, A. Gloter, D. Imhoff, C. Deranlot, N. D. Mathur, S. Fusil, K. Bouzehouane and A. Barthélémy, *Science*, 2010, **327**, 1106.
7. Z. Wen, C. Li, D. Wu, A. D. Li and N. B. Ming, *Nature Mater.*, 2013, **12**, 617.
8. M. Gajek, M. Bibes, S. Fusil, K. Bouzehouane, J. Fontcuberta, A. Barthélémy and A. Fert, *Nature Mater.*, 2007, **6**, 296.
9. J. P. Velev, C. G. Duan, J. D. Burton, A. Smogunov, M. K. Niranjan, E. Tosatti, S. S. Jaswal and E. Y. Tsymbal, *Nano Lett.*, 2009, **9**, 427.
10. S. M. Wu, S. A. Cybart, P. Yu, M. D. Rossell, J. X. Zhang, R. Ramesh and R. C. Dynes, *Nature Mater.*, 2010, **9**, 756.
11. K. Yoshida, I. Hamada, S. Sakata, A. Umeno, M. Tsukada, K. Hirakawa, *Nano Lett.*, 2013, **13**, 481.
12. M. Prezioso, A. Riminucci, I. Bergenti, P. Graziosi, D. Brunel and V. A. Dediu, *Adv. Mater.*, 2011, **23**, 1371.
13. J. J. Yang, M. D. Pickett, X. Li, D. A. A. Ohlberg, D. R. Stewart and R. S. Williams, *Nature Nanotech.*, 2008, **3**, 429.
14. F. Bonell, Y. T. Takahashi, D. D. Lam, S. Yoshida, Y. Shiota, S. Miwa, T. Nakamura and Y. Suzuki, *Appl. Phys. Lett.*, 2013, **102**, 152401.
15. N. Izyumskaya, Y. Alivov and H. Morkoc, *Crit. Rev. Solid State Mat. Sci.*, 2009, **34**, 89.
16. J. Y. Son, Y. H. Shin, H. Kim and H. M. Jang, *ACS Nano*, 2010, **4**, 2655.
17. A. Sawa, *Materials Today*, 2008, **11**, 28.
18. E. Y. Tsymbal, O. N. Mryasov and P. R. LeClair, *J. Phys.: Cond. Mater.*, 2003, **15**, R109.
19. Q. Li, T. T. Shen, Y. L. Cao, K. Zhang, S. S. Yan, Y. F. Tian, S. S. Kang, M. W. Zhao, Y. Y. Dai, Y. X. Chen, G. L. Liu, L. M. Mei, X. L. Wang and P. Grünberg, *Scientific Reports*, 2014, **4**, 3835
20. G. Kresse and J. Furthmüller, *Phys. Rev. B*, 1996, **54**, 11169.
21. S. L. Dudarev, G. A. Botton, S. Y. Savrasov, C. J. Humphreys and A. P. Sutton, *Phys. Rev. B*, 1998, **57**, 1505.
22. S. Grytsyuk, M. V. Peskov and U. Schwingenschlögl, *Phys. Rev. B*, 2012, **86**, 174115.
23. Y. Zhao, T. E. Feltes, J. R. Regalbuto, R. J. Meyer and R. F. Klie, *J. Appl. Phys.*, 2010, **108**, 063704.
24. M. Julliére, *Phys. Lett. A*, 1975, **54**, 225.
25. J. Bass and W. P. Pratt, *J. Magn. Magn. Mater.*, 1999, **200**, 274.
26. W. H. Meiklejohn and C. P. Bean, *Phys. Rev.*, 1956, **102**, 1413.
27. J. S. Moodera and G. Mathon, *J. Magn. Magn. Mater.*, 1999, **200**, 248.
28. J. Camarero, J. Sort, A. Hoffman, J. M. García-Martín, B. Dieny, R. Miranda and J. Nogués, *Phys. Rev. Lett.*, 2005, **95**, 057204.
29. H. Zare-Kolsaraki and H. Micklitz, *Phys. Rev. B*, 2003, **67**, 224427.
30. P. LeClair, J. K. Ha, H. J. M. Swagten, J. T. Kohlhepp, C. H. VandeVin and W. J. W. DeJonge, *Appl. Phys. Lett.*, 2002, **80**, 625.
31. S. Mitani, S. Takahashi, K. Takanashi, K. Yakushiji, S. Maekawa and H. Fujimori, *Phys. Rev. Lett.*, 1998, **81**, 2799.
32. G. Schmidt, D. Ferrand, L. W. Molenkamp, A. T. Filip and B. J. Vanwees, *Phys. Rev. B*, 2000, **62**, R4790.